

Narrow-linewidth tin-vacancy centers in a diamond waveguide

Alison E. Rugar,^{*,†,#} Constantin Dory,^{†,#} Shahriar Aghaeimeibodi,^{†,#} Haiyu Lu,^{‡,¶}
 Shuo Sun,[†] Sattwik Deb Mishra,[†] Zhi-Xun Shen,^{‡,§,¶,||} Nicholas A. Melosh,^{||,⊥,¶}
 and Jelena Vučković[†]

[†]*E. L. Ginzton Laboratory, Stanford University, Stanford, CA 94305, USA*

[‡]*Department of Physics, Stanford University, Stanford, California 94305, United States*

[¶]*Geballe Laboratory for Advanced Materials, Stanford University, Stanford, California 94305, United States*

[§]*Department of Applied Physics, Stanford University, Stanford, California 94305, United States*

^{||}*Stanford Institute for Materials and Energy Sciences, SLAC National Accelerator Laboratory, Menlo Park, California 94025, United States*

[⊥]*Department of Materials Science and Engineering, Stanford University, Stanford, California 94305, United States*

[#]*These authors contributed equally to this work.*

E-mail: arugar@stanford.edu

Abstract

Integrating solid-state quantum emitters with photonic circuits is essential for realizing large-scale quantum photonic processors. Negatively charged tin-vacancy (SnV^-) centers in diamond have emerged as promising candidates for quantum emitters because

of their excellent optical and spin properties including narrow-linewidth emission and long spin coherence times. SnV^- centers need to be incorporated in optical waveguides for efficient on-chip routing of the photons they generate. However, such integration has yet to be realized. In this Letter, we demonstrate the coupling of SnV^- centers to a nanophotonic waveguide. We realize this device by leveraging our recently developed shallow ion implantation and growth method for generation of high-quality SnV^- centers and the advanced quasi-isotropic diamond fabrication technique. We confirm the compatibility and robustness of these techniques through successful coupling of narrow-linewidth SnV^- centers (as narrow as 34 ± 4 MHz) to the diamond waveguide. Our results are an important step toward SnV^- -based on-chip spin-photon interfaces, single-photon nonlinearity, and photon-mediated spin interactions.

Keywords

Tin-vacancy center, color centers, diamond fabrication, waveguides, quantum photonics, shallow ion implantation and growth

Introduction

The realization of large-scale optical quantum information processing requires the integration of quantum emitters into a photonic infrastructure that guides and manipulates light.¹ In recent years, several color centers in solids have been explored as potential optically interfaced qubit candidates.² In particular, group-IV color centers in diamond, such as the negatively charged silicon-,³⁻⁵ germanium-,⁶⁻⁸ tin-,⁹⁻¹³ and lead-vacancy^{14,15} (SiV^- , GeV^- , SnV^- , and PbV^- respectively) centers have garnered much attention because of their favorable optical properties and robustness to electric-field fluctuations to first order, due in large part to their inversion-symmetric structure.^{16,17} While remarkable progress has been made in SiV^- and GeV^- quantum photonics,¹⁸⁻²¹ it is important to extend those efforts to other color centers

with comparable or superior properties in order to find the best possible qubit candidate. The SnV^- center is of specific interest because it is expected to have long spin coherence times at temperatures above 1 K,^{13,22} unlike the negatively charged SiV^- and GeV^- centers which require dilution refrigerator temperatures.¹⁷ However, despite its exciting potential as an optically interfaced qubit candidate, the SnV^- center has not yet been incorporated into any nanophotonic devices that can be scaled to eventually form integrated quantum photonic circuits.

In this paper, we present the first demonstration of SnV^- centers coupled to a waveguide, a fundamental building block for waveguide quantum electrodynamics^{20,23,24} and large-scale photonic circuitry. SnV^- centers are generated via the shallow ion implantation and growth (SIIG) method,²⁵ and the waveguide is fabricated using a quasi-isotropic etch technique.^{26–29} The measured linewidth of a resulting SnV^- center coupled to a waveguide in our sample is on par with those measured in previous reports of lifetime-limited SnV^- centers.^{13,30} The previously characterized SnV^- centers were either in bulk diamond³⁰ or micropillars¹³ and were generated via high-energy implantation and annealing in vacuum¹³ or high-pressure, high-temperature (HPHT) environments.³⁰ Our results demonstrate that the SIIG method and fabrication based on a quasi-isotropic undercut can be combined to form a platform for quantum photonics experiments with high-quality SnV^- centers. Having narrow-linewidth SnV^- centers in nanophotonic structures in diamond paves the way to more advanced on-chip quantum optics experiments performed at higher temperatures than previously allowed by the SiV^- center.

Sample preparation

An electronic grade diamond chip from ElementSix is first cleaned in a boiling tri-acid solution consisting of nitric, sulfuric, and perchloric acids in equal part. The top ~ 500 nm of the diamond chip is then removed via an oxygen (O_2) plasma etch. The subsequent color

center generation and nanofabrication steps are detailed below and illustrated schematically in Fig. 1.

SnV^- centers are generated on the chip via the shallow ion implantation and growth (SIIG) method.²⁵ The prepared chip is implanted by CuttingEdge Ions with $^{120}\text{Sn}^+$ ions at 1 keV and a dose of $1.6 \times 10^{10} \text{ cm}^{-2}$. The implanted chip is then cleaned with a hydrogen (H_2) plasma immediately before 90 nm of diamond is grown via microwave-plasma chemical vapor deposition (MPCVD, Seki Diamond Systems SDS 5010) as detailed in Ref. 25.

With SnV^- centers embedded 90 nm below the diamond surface, we fabricate suspended bare waveguides. We first grow 200 nm of Si_xN_y via plasma-enhanced chemical vapor deposition (PECVD) to serve as an etch mask (Fig. 1(d)). We define the structures in hydrogen silsesquioxane FOx-16 via electron-beam lithography and transfer the pattern into the Si_xN_y with a SF_6 , CH_4 , and N_2 reactive ion etch (RIE) (Fig. 1(e)). With the Si_xN_y etch mask patterned, we then etch the diamond with an anisotropic O_2 RIE (Fig. 1(f)). Next, 30 nm of Al_2O_3 are grown via atomic layer deposition (Fig. 1(g)). The horizontal planes of the Al_2O_3 layer are removed with a Cl_2 , BCl_2 , and N_2 RIE (Fig. 1(h)). A second anisotropic O_2 RIE is performed to expose part of the vertical sidewalls of the diamond structure (Fig. 1(i)). The quasi-isotropic etch^{26–29} step can now be performed to undercut the structures (Fig. 1(j)). To do so, the forward bias of the O_2 RIE is turned off, and the etch is performed at high temperature with high inductively coupled plasma power.^{26–29} The resulting etch progresses preferentially along the $\{110\}$ planes.²⁶ When the nanobeam waveguides have been released (Fig. 1(k)) and have been etched to the desired thickness, as validated by high-voltage SEM imaging, the sample is soaked in hydrofluoric acid to remove the Si_xN_y and Al_2O_3 etch masks (Fig. 1(l)).

The resulting waveguides are 400 nm wide, 10 μm long, and 280 nm thick. On either end of the waveguides is an inverse-designed^{29,31} vertical coupler (VC) to couple incident light from free space into the waveguide and vice versa. A typical scanning electron microscope (SEM) image of a resulting nanostructure is shown in Fig. 1(m). We note that the waveguide

structures that we use for our measurements are solid nanobeams with VCs and without the photonic crystal.

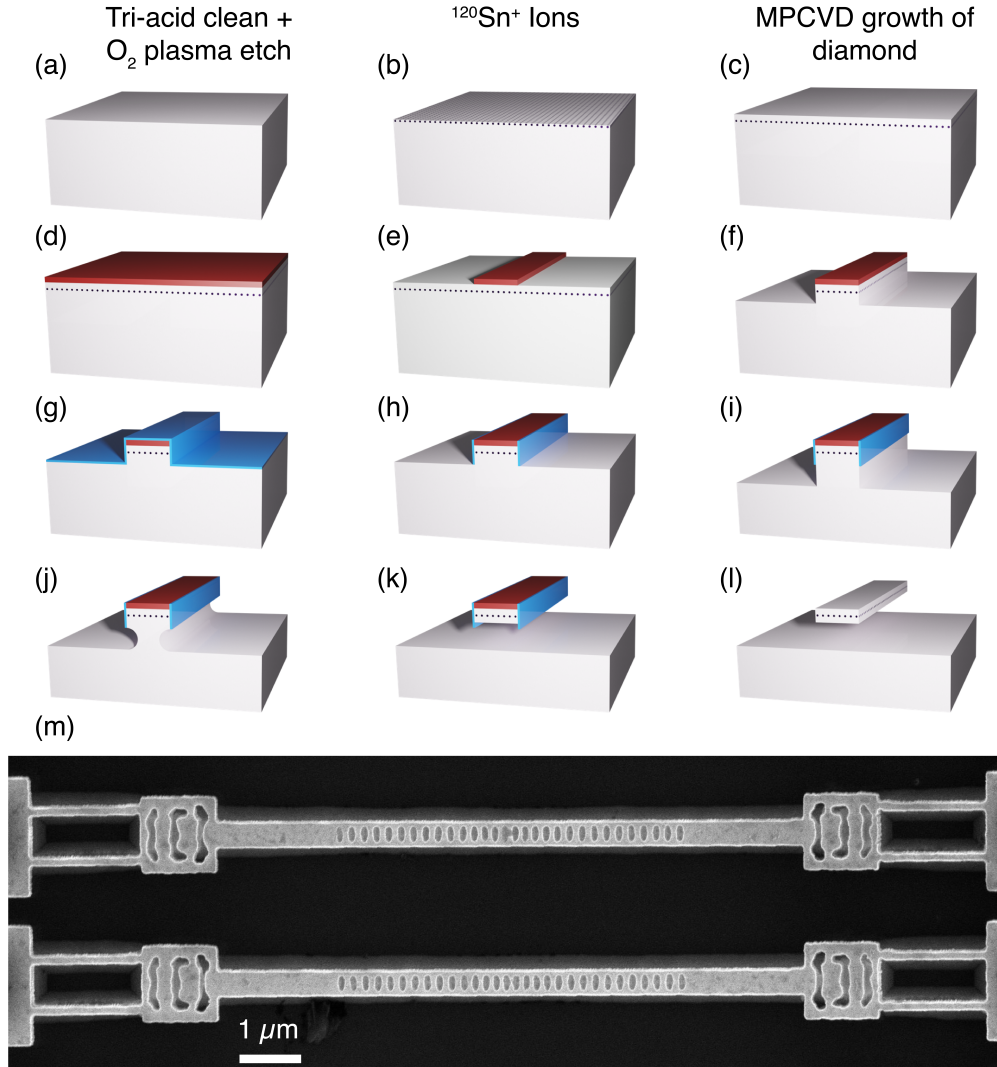


Figure 1: Sample fabrication. (a)–(l) Schematics of sample fabrication. (a) Tri-acid clean and etch of electronic grade diamond with O₂ plasma. (b) Implantation of ¹²⁰Sn⁺ ions at 1 keV with a dose of $1.6 \times 10^{10} \text{ cm}^{-2}$. (c) H₂ plasma clean and MPCVD growth of 90 nm of diamond. (d) PECVD growth of 200 nm of Si_xN_y (red) as an etch mask. (e) Electron-beam lithography and SF₆, CH₄, and N₂ RIE to transfer pattern to the Si_xN_y etch mask. (f) Anisotropic O₂ dry etch of diamond. (g) Atomic layer deposition of 30 nm of Al₂O₃ (blue). (h) Anisotropic dry etch of Al₂O₃. (i) Second anisotropic O₂ dry etch of diamond. (j) Quasi-isotropic etch of diamond along the {110} facet allows the undercut to form. (k) Continuation of quasi-isotropic etch until desired thickness is attained. Higher etch rate along {110} compared to {001} leads to a flat bottom surface. (l) Removal of Si_xN_y and Al₂O₃ masks. (m) Typical SEM image of resulting devices.

Results and discussion

Photoluminescence map

To characterize the fabricated devices, we use two home-built cryogenic setups. First, we acquire two-dimensional photoluminescence (PL) maps of potential structures using a scanning confocal microscope operating at 5 K. In this setup, an objective lens inside the cryostat (Montana Instruments) focuses a continuous-wave laser at 532 nm on the sample to excite the emitters non-resonantly. The emitted photons are collected using the same objective lens and a single-mode fiber. We spectrally filter the collected light using a 568-nm long-pass filter and sent the filtered signal to a single-photon counting module. A typical resulting PL map of a nanobeam waveguide on this sample is shown in Fig. 2(a). The high counts and distinct bright spots apparent on the device in the PL map indicate the existence of SnV^- centers in the nanobeam. PL spectroscopy is next used to confirm the presence of SnV^- centers in the devices.

Photoluminescence excitation

To characterize the linewidth of the emitters, we move to another cryostat (attoDRY2100) that operates at 1.7 K. We first collect a PL spectrum, shown in Fig. 2(b) by focusing a 532-nm laser on a spot in the middle of the waveguide, collecting the emitted light from the same spot with a multimode fiber, and sending the collected light to a spectrometer. This spectrum displays multiple distinct zero-phonon lines, indicating that multiple SnV^- centers are present in the nanobeam waveguide.

We perform photoluminescence excitation (PLE) on a color center in the same waveguide. We scan the wavelength of the MSquared External Mixing Module around the resonant wavelength of the color center of interest. Counting photons emitted into the phonon sideband of the SnV^- center, we observe a peak in emission as the laser crosses resonance with the color center and thus can infer the linewidth of the color center. We perform PLE

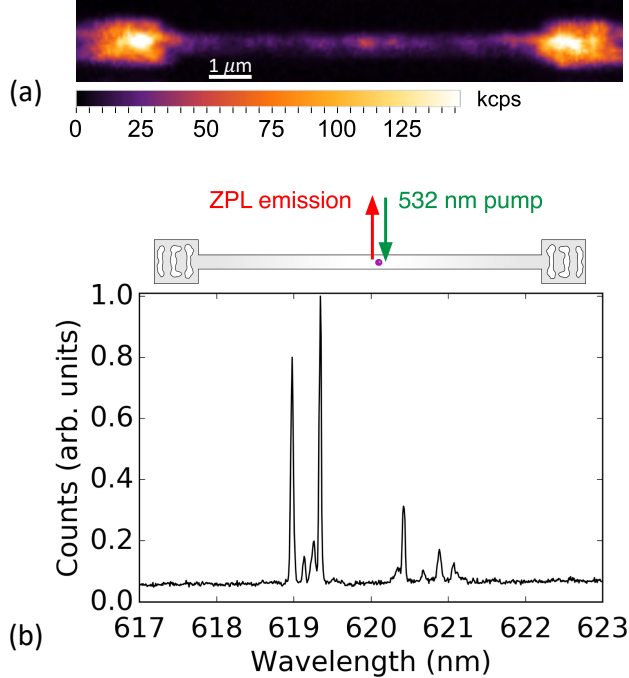


Figure 2: PL of SnV^- centers in a waveguide. (a) PL map of a waveguide on the chip containing SnV^- centers. (b) PL spectrum collected on a waveguide with excitation and collection (MM fiber) aligned on the same spot. The configuration is shown schematically above the plot.

in two configurations: top-down and VC-to-VC. In the former, illustrated schematically in Fig. 3(a), the excitation laser is coupled out of a single-mode polarization maintaining fiber and is focused on a spot on the waveguide. The collection fiber is aligned to the same spot on the waveguide. In the VC-to-VC configuration, illustrated schematically in Fig. 3(b), the excitation spot is focused on one VC. The emission is collected from the opposite VC. In both configurations, the emitted light is passed through a 638-nm long-pass filter and a 700-nm short-pass filter before being collected by a multimode fiber.

Figs. 3(a) and (b) display the resulting data for the top-down and VC-to-VC configurations respectively. The different passes of the laser through resonance are offset in the plot for clarity, with the lowest scan being the first. In both configurations, multiple peaks are apparent in several scans but not all appear in the same scans. The many peaks in Fig. 3(b) may indicate that several emitters are coupled to the waveguide, as expected from the PL shown in Fig. 2. The inconsistent appearances of some peaks may indicate instabilities in

the charge states of those emitters. The fact that these instabilities are observed in both configurations further confirms that this is a color-center-related phenomenon rather than a waveguide-related one. Similar observations have been reported in Ref. 30 where SnV^- centers were generated via high-energy ion implantation and HPHT annealing. Further experimental efforts are required to understand and to mitigate the source of instability in the emission spectra of the SnV^- emitters.

From the data in Figs. 3(a) and (b), we fit a Lorentzian to one peak for each configuration, indicated by a red arrow. The Lorentzian fit to these data, shown in Figs. 3(c) and (d), reveals linewidths of 29 ± 5 MHz and 34 ± 4 MHz respectively. Notably, both of these linewidths are comparable to previously reported lifetime-limited linewidths^{13,30} despite several fabrication steps performed on this sample. The ability to produce narrow-linewidth SnV^- centers in suspended waveguides will enable the future fabrication of large-scale photonic circuitry and quantum photonics experiments.

Conclusion and outlook

In this work we have integrated narrow-linewidth SnV^- centers in diamond nanobeam waveguides. These results indicate that the combination of the SIIG method²⁵ and the quasi-isotropic undercut^{26–29} forms a promising platform for future quantum photonics with the SnV^- center. For example, carefully optimizing the coupling efficiency of the narrow-linewidth emitter to the waveguide mode enables a broadband interface for spin-controlled photon switching³² and few-photon nonlinearity.³³

To go beyond single-emitter experiments, deterministic positioning of the SnV^- centers along the waveguide is essential. Fortunately, as previously demonstrated in Ref. 25, we can achieve site-controlled generation of SnV^- centers with an implantation mask defined with standard lithography. Deterministic positioning combined with small inhomogeneous broadening of SnV^- centers will enable the coupling of multiple identical emitters to the

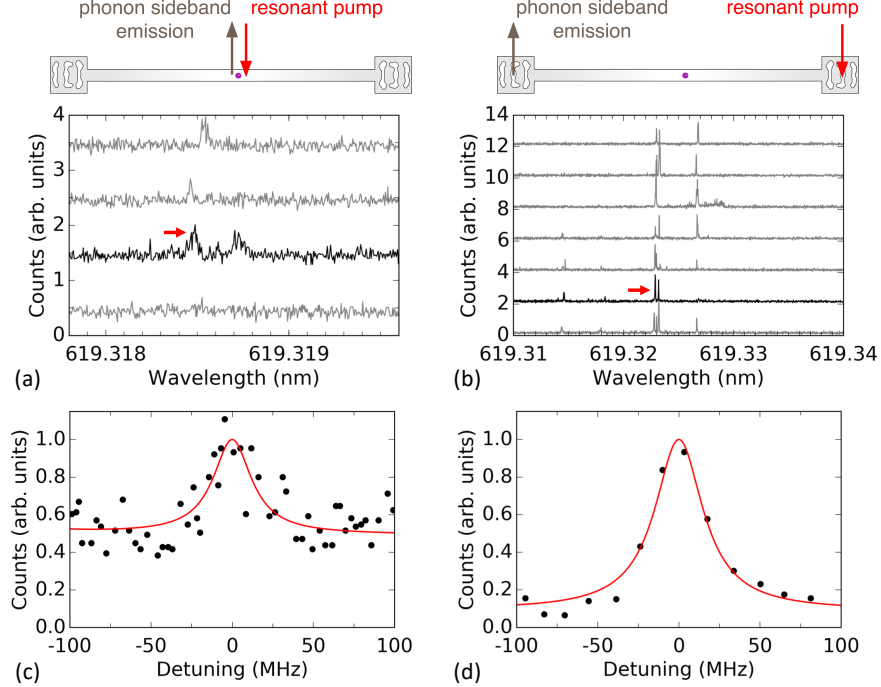


Figure 3: PLE of a SnV^- center in a waveguide. (a) PLE scans in the top-down configuration, as shown schematically above the plot. Repeated scans are offset vertically for clarity. A few distinct peaks are visible but do not always appear. (b) PLE scans in the VC-to-VC configuration, as shown schematically above the plot. Repeated scans are offset vertically for clarity. Several distinct peaks are visible, but not all peaks are consistently apparent. The red arrows in (a) and (b) indicate a peak that we investigate more closely in the next panels. (c) Close-up view of the peak indicated by the red arrow in (a). A Lorentzian fit (red curve) to the data (black dots) reveals a linewidth of 29 ± 5 MHz. (d) Close-up view of the peak indicated by the red arrow in (b). A Lorentzian fit (red curve) to the data (black dots) reveals a linewidth of 34 ± 4 MHz.

same optical mode for superradiance and quantum few-body experiments.^{23,24,34}

Moreover, having high-quality SnV^- centers in suspended nanophotonic structures in diamond enables the future integration of the color centers into cavities to enhance the spin-photon interaction. Ultimately, such devices will be beneficial for several quantum information applications and can operate at elevated temperatures compared to previous demonstrations with SiV^- centers.¹⁹

Acknowledgement

This work is financially supported by Army Research Office (ARO) (award no. W911NF-13-1-0309); National Science Foundation (NSF) RAISE TAQS (award no. 1838976); Air Force Office of Scientific Research (AFOSR) DURIP (award no. FA9550-16-1-0223); Department of Energy, Basic Energy Sciences (BES) - Materials Science and Engineering; and SLAC LDRD. A.E.R. acknowledges support from the National Defense Science and Engineering Graduate (NDSEG) Fellowship Program, sponsored by the Air Force Research Laboratory (AFRL), the Office of Naval Research (ONR) and the Army Research Office (ARO). C.D. acknowledges support from the Andreas Bechtolsheim Stanford Graduate Fellowship and the Microsoft Research PhD Fellowship. S.A. acknowledges support from Stanford Q-FARM postdoctoral fellowship. Part of this work was performed at the Stanford Nanofabrication Facility (SNF) and the Stanford Nano Shared Facilities (SNSF), supported by the National Science Foundation under award ECCS-1542152.

References

- (1) Kimble, H. J. The quantum internet. *Nature* **2008**, *453*, 1023–1030.
- (2) Awschalom, D. D.; Hanson, R.; Wrachtrup, J.; Zhou, B. B. Quantum technologies with optically interfaced solid-state spins. *Nat. Photon.* **2018**, *12*, 516–27.
- (3) Neu, E.; Steinmetz, D.; Riedrich-Möller, J.; Gsell, S.; Fischer, M.; Schreck, M.; Becher, C. Single photon emission from silicon-vacancy colour centres in chemical vapour deposition nano-diamonds on iridium. *New J. Phys.* **2011**, *13*, 025012.
- (4) Hepp, C.; Müller, T.; Waselowski, V.; Becker, J. N.; Pingault, B.; Sternschulte, H.; Steinmüller-Nethl, D.; Gali, A.; Maze, J. R.; Atatüre, M.; Becher, C. Electronic Structure of the Silicon Vacancy Color Center in Diamond. *Phys. Rev. Lett.* **2014**, *112*, 036405.

- (5) Müller, T.; Hepp, C.; Pingault, B.; Neu, E.; Gsell, S.; Schreck, M.; Sternschulte, H.; Steinmüller-Nethl, D.; Becher, C.; Atatüre, M. Optical signatures of silicon-vacancy spins in diamond. *Nat. Commun.* **2014**, *5*, 3328.
- (6) Iwasaki, T. et al. Germanium-Vacancy Single Color Centers in Diamond. *Sci. Rep.* **2015**, *5*, 12882.
- (7) Palyanov, Y. N.; Kupriyanov, I. N.; Borzdov, Y. M.; Surovtsev, N. V. Germanium: a new catalyst for diamond synthesis and a new optically active impurity in diamond. *Sci. Rep.* **2015**, *5*, 14789.
- (8) Ekimov, E. A.; Lyapin, S. G.; Boldyrev, K. N.; Kondrin, M. V.; Khmel'nitskiy, R.; Gavva, V. A.; Kotereva, T. V.; Popova, M. N. Germanium-Vacancy Color Center in Isotopically Enriched Diamonds Synthesized at High Pressures. *JETP Lett.* **2015**, *102*, 701–706.
- (9) Iwasaki, T.; Miyamoto, Y.; Taniguchi, T.; Siyushev, P.; Metsch, M. H.; Jelezko, F.; Hatano, M. Tin-Vacancy Quantum Emitters in Diamond. *Phys. Rev. Lett.* **2017**, *119*, 253601.
- (10) Tchernij, S. D.; Herzig, T.; Forneris, J.; Küpper, J.; Pezzagna, S.; Train, P.; Morev, E.; Brida, I. P. D. G.; Skukan, N.; Genovese, M.; Jakšić, M.; Meijer, J.; Olivero, P. Single-Photon-Emitting Optical Centers in Diamond Fabricated upon Sn Implantation. *ACS Photonics* **2017**, *4*, 2580–6.
- (11) Ekimov, E. A.; Lyapin, S. G.; Kondrin, M. V. Tin-vacancy color centers in micro- and polycrystalline diamonds synthesized at high pressures. *Diam. Relat. Mater.* **2018**, *87*, 223–7.
- (12) Rugar, A. E.; Dory, C.; Sun, S.; Vučković, J. Characterization of optical and spin properties of single tin-vacancy centers in diamond nanopillars. *Phys. Rev. B* **2019**, *99*, 205417.

- (13) Trusheim, M. E. et al. Transform-Limited Photons From a Coherent Tin-Vacancy Spin in Diamond. *Phys. Rev. Lett.* **2020**, *124*, 023602.
- (14) Trusheim, M. E.; Wan, N. H.; Chen, K. C.; Ciccarino, C. J.; Flick, J.; Sundararaman, R.; Malladi, G.; Bersin, E.; Walsh, M.; Lienhard, B.; Bakhru, H.; Narang, P.; Englund, D. Lead-related quantum emitters in diamond. *Phys. Rev. B* **2019**, *99*, 075430.
- (15) Tchernij, S. D. et al. Single-Photon Emitters in Lead-Implanted Single-Crystal Diamond. *ACS Photonics* **2018**, *5*, 4864–71.
- (16) Evans, R. E.; Sipahigil, A.; Sukachev, D. D.; Zibrov, A. S.; Lukin, M. D. Narrow-Linewidth Homogeneous Optical Emitters in Diamond Nanostructures via Silicon Ion Implantation. *Phys. Rev. Applied* **2016**, *5*, 044010.
- (17) Bradac, C.; Gao, W.; Forneris, J.; Trusheim, M.; Aharonovich, I. Quantum nanophotonics with group IV defects in diamond. *Nat. Commun.* **2019**, *10*, 5625.
- (18) Nguyen, C. T.; Sukachev, D. D.; Bhaskar, M. K.; Machielse, B.; Levonian, D. S.; Knall, E. N.; Stroganov, P.; Riedinger, R.; Park, H.; Lončar, M.; Lukin, M. D. Quantum Network Nodes Based on Diamond Qubits with an Efficient Nanophotonic Interface. *Phys. Rev. Lett.* **2019**, *123*, 183602.
- (19) Bhaskar, M. K.; Riedinger, R.; Machielse, B.; Levonian, D. S.; Nguyen, C. T.; Knall, E. N.; Park, H.; Englund, D.; Lončar, M.; Sukachev, D. D.; Lukin, M. D. Experimental demonstration of memory-enhanced quantum communication. *Nature* **2020**, *580*, 60–64.
- (20) Bhaskar, M. K.; Sukachev, D. D.; Sipahigil, A.; Evans, R. E.; Burek, M. J.; Nguyen, C. T.; Rogers, L. J.; Siyushev, P.; Metsch, M. H.; Park, H.; Jelezko, F.; Lončar, M.; Lukin, M. D. Quantum Nonlinear Optics with a Germanium-Vacancy Color Center in a Nanoscale Diamond Waveguide. *Phys. Rev. Lett.* **2017**, *118*, 223603.

- (21) Bray, K.; Regan, B.; Trycz, A.; Previdi, R.; Seniutinas, G.; Ganesan, K.; Kianinia, M.; Kim, S.; Aharonovich, I. Single Crystal Diamond Membranes and Photonic Resonators Containing Germanium Vacancy Color Centers. *ACS Photonics* **2018**, *5*, 4817–22.
- (22) Thiering, G.; Gali, A. *Ab Initio* Magneto-Optical Spectrum of Group-IV Vacancy Color Centers in Diamond. *Phys. Rev. X* **2018**, *8*, 021063.
- (23) Sipahigil, A. et al. An integrated diamond nanophotonics platform for quantum-optical networks. *Science* **2016**, *354*, 847–50.
- (24) Grim, J. Q.; Bracker, A. S.; Zalalutdinov, M.; Carter, S. G.; Kozen, A. C.; Kim, M.; Kim, C. S.; Mlack, J. T.; Yakes, M.; Lee, B.; Gammon, D. Scalable in operando strain tuning in nanophotonic waveguides enabling three-quantum-dot superradiance. *Nat. Mater.* **2019**, *18*, 963–969.
- (25) Rugar, A. E.; Lu, H.; Dory, C.; Sun, S.; McQuade, P. J.; Shen, Z.-X.; Melosh, N. A.; Vučković, J. Generation of Tin-Vacancy Centers in Diamond via Shallow Ion Implantation and Subsequent Diamond Overgrowth. *Nano Lett.* **2020**, *20*, 1614–1619.
- (26) Mouradian, S.; Wan, N. H.; Schröder, T.; Englund, D. Rectangular photonic crystal nanobeam cavities in bulk diamond. *Appl. Phys. Lett.* **2017**, *111*, 021103.
- (27) Wan, N. H.; Mouradian, S.; Englund, D. Two-dimensional photonic crystal slab nanocavities on bulk single-crystal diamond. *Appl. Phys. Lett.* **2018**, *112*, 141102.
- (28) Mitchell, M.; Lake, D. P.; Barclay, P. E. Realizing $Q > 300\,000$ in diamond microdisks for optomechanics via etch optimization. *APL Photonics* **2019**, *4*, 016101.
- (29) Dory, C.; Vercrusse, D.; Yang, K. Y.; Sapra, N. V.; Rugar, A. E.; Sun, S.; Lukin, D. M.; Piggott, A. Y.; Zhang, J. L.; Radulaski, M.; Lagoudakis, K. G.; Su, L.; Vučković, J. Inverse-designed diamond photonics. *Nat. Commun.* **2019**, *10*, 3309.

- (30) Görlitz, J.; Herrmann, D.; Thiering, G.; Fuchs, P.; Gandil, M.; Iwasaki, T.; Taniguchi, T.; Kieschnick, M.; Meijer, J.; Hatano, M.; Gali, A.; Becher, C. Spectroscopic investigations of negatively charged tin-vacancy centres in diamond. *New J. Phys.* **2020**, *22*, 013048.
- (31) Molesky, S.; Lin, Z.; Piggott, A. Y.; Jin, W.; Vučković, J.; Rodriguez, A. W. Inverse design in nanophotonics. *Nat. Photon.* **2018**, *12*, 659–670.
- (32) Javadi, A. et al. Spin–photon interface and spin-controlled photon switching in a nanobeam waveguide. *Nat. Nanotechnol.* **2018**, *13*, 398–403.
- (33) Thyrrstrup, H. et al. Quantum Optics with Near-Lifetime-Limited Quantum-Dot Transitions in a Nanophotonic Waveguide. *Nano Lett.* **2018**, *18*, 1801–1806.
- (34) Kim, J.-H.; Aghaeimeibodi, S.; Richardson, C. J. K.; Leavitt, R. P.; Waks, E. Super-Radiant Emission from Quantum Dots in a Nanophotonic Waveguide. *Nano Lett.* **2018**, *18*, 4734.